Theory and experiment for the reaction ^{6}Li$(e, d)e', ^4$He†

D. M. Skopik, E. L. Tomusiak, E. T. Dressler, Y. M. Shin, and J. J. Murphy, II
Saskatchewan Accelerator Laboratory, University of Saskatchewan, Saskatoon, Canada S7N 0W0
(Received 26 April 1976)

Deuterons from the reaction ^{6}Li$(e, d)e', ^4$He were measured at eight laboratory angles over a deuteron energy interval of approximately 2–10 MeV. The incident electron energy was chosen so that only deuterons and α particles were left in the final state. These data are compared to a one-resonance square-well electrodisintegration model. Extracted photodisintegration cross sections are also compared with a more sophisticated Woods-Saxon photodisintegration theory. In both comparisons the data and theory are in overall qualitative agreement.

[NUCLEAR REACTIONS ^{6}Li$(e, d)e', ^4$He, measured $\sigma(E_d, \theta_d)$, $E_d \simeq 2$–10 MeV, $\theta = 30$–150°, extracted ^{6}Li$(\gamma, d)^4$He for $E_x > 10$ MeV.]

I. INTRODUCTION

The detailed structure (J^π, E_x, and Γ of the resonances) of ^{6}Li has been reasonably well established by electron and nucleon scattering experiments.[1] In addition, a number of theoretical treatments have been carried out for ^{6}Li, with perhaps the most physically intuitive of these being the α-deuteron cluster model. Indeed, the most recent inelastic electron scattering experiment below the (γ, p) threshold[2] reports quite good agreement with an α-d cluster calculation employing a Woods-Saxon potential that contained two of the L-S coupled states at 2.185 and 4.31 MeV.

Photodisintegration or capture measurements in the α-d channel on the other hand have not been performed in overwhelming numbers. This is due mainly to the fact that the reaction is primarily $E2$, since the center of mass and center of charge of the α-deuteron pair are nearly coincident. This $E2$ nature of the reaction results in a very low counting rate for the experiment. However, there are a number of features of this reaction channel that are interesting enough to stimulate some new measurements. These features are that: (a) while the α-d cluster model has successfully explained a large body of scattering data, a more satisfactory test of the theory will arise in comparing the model predictions to a measurement of one of the disintegrated clusters; (b) since $E1$ transitions are not strictly forbidden, the angular distribution of the emitted particles should not be pure $\sin^2\theta\cos^2\theta$, but rather be slightly isotropic and asymmetric where the $E1$ contribution is not negligible; (c) in an α-d cluster model which assumes that the ground state of ^{6}Li is pure $^3S_1$, $M1$ spin-flip transitions are forbidden in the reaction ^{6}Li$(\gamma, d)^4$He, therefore the importance of higher order terms in the $M1$ transition operator and/or $L = 2$ admixtures in the ground state perhaps could be determined; (d) if the α-d states in ^{6}Li are not pure $T = 0$ states, small $T = 1$ admixtures could influence the predictions of the models.

II. EXPERIMENTAL

The experimental arrangement for measuring deuterons following electron bombardment of ^{6}Li is composed of the University of Saskatchewan linear accelerator and a positive ion spectrometer. The accelerator and spectrometer have been described elsewhere.[3] Briefly, the spectrometer is a 127° double-focusing magnet equipped with an array of five surface barrier silicon detectors. The signals from these detectors were fed to analog to digital converters (ADC) interfaced to an XDS computer. The ADC's were gated by the accelerator master trigger to reduce the background. A sliding vacuum seal allowed the spectrometer to be positioned at any angle between 27° and 155°. The calibration of the spectrometer described in Ref. 4 consists of measuring the energy response and efficiency of each detector and the solid angle of the spectrometer with a known α source. These calibrations have been checked by measuring the recoil protons from the elastic reaction $H(e, H')e'$ at a number of different proton recoil energies. The number of electrons incident on the target was measured by a nonintercepting ferrite monitor designed at SLAC. The ferrite monitor was periodically checked against a Faraday cup for stability and linearity. The total error assigned to these calibrations is ±5%.

Since the magnet holds the ratio of particle momentum to charge constant for a given magnetic field, the deuterons could easily be distinguished from the other emitted particles, an experimental feature not present in earlier measurements of this reaction. Figure 1 is one of the better spectra

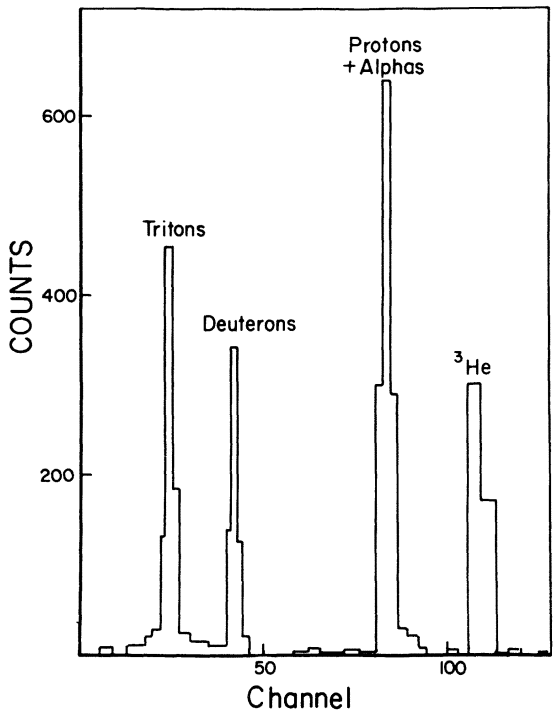

FIG. 1. Pulse height spectrum showing all mass groups that result from the disintegration of ^{6}Li.

which shows clearly the large separation between the deuterons and other mass groups. The deuteron peaks were integrated and charge normalized on line. The initial data analysis, consisting of weighting and combining all data taken at the same incident energy and angle, was also performed on line. The remaining data analysis, energy loss corrections, least squares fitting, etc., was done off line. The final electrodisintegration cross section is then given by

$$\frac{d^2\sigma}{d\Omega_d dE_d} = \frac{C_d(\theta_d, E_d)}{\Delta\Omega \Delta E_d \eta_t(\theta)} , \tag{1}$$

where $C_d(\theta_d, E_d)$ is the charge normalized deuteron yield, $\Delta\Omega$ and $\Delta E_d = 0.001\,26 E_d$ are the solid angle and energy bite of the spectrometer, and $\eta_t(\theta)$ is the number of target nuclei per cm^2.

This cross section can now be compared directly with theory if the theory incorporates an integration over all possible final electron states. In practice this integration, while time consuming, is not difficult. Also, because the electrodisintegration is weighted by q_μ^{-4}, where q_μ is the four-momentum transfer, an approximate excitation energy in ^{6}Li can also be computed. This comparison has the advantage that a "virtual photon spectrum" does not have to be introduced in the data analysis, but to date few electrodisintegration calculations have been carried out.

If on the other hand a comparison with real photon experiments or theory is desired, an equivalent photodisintegration cross section can be obtained using virtual photon theory. In practice, where the $E1$ cross section is dominant one can simply divide by the $E1$ photon spectrum and use the resulting cross sections as equivalent photodisintegration data. As pointed out in Ref. 5, this procedure (when $E1$ is dominant) introduces very little error compared to the complete treatment in which the multipolarity dependence of the virtual photon spectrum is taken into account. For ^{6}Li, however, the photodisintegration cross section is predominantly $E2$, and since in the long wave limit the $E0$ and $E2$ matrix elements are of the same order of magnitude (the $E0$ is present when electrons rather than photons are used to initiate the reaction), the extraction of a photodisintegration cross section is valid only when kinematic conditions are such that the $E0$ contribution to the virtual photon spectrum is negligible (see Ref. 5).

In the present experiment these kinematic conditions are not met very well for the excitation energies that have investigated, but nevertheless some statements about the equivalent photodisintegration cross section can still be made. First, by neglecting the $E0$ photon spectrum the magnitude of the photon cross section is overestimated and is thus an upper limit, and secondly, the angular distributions should reflect the $E2$ character of the transition but be more isotropic due to the presence of $E0$ strength. In the extraction of the equivalent photodisintegration cross section we have limited the excitation energy in ^{6}Li to values greater than 10 MeV. This corresponds (by examining the electrodisintegration calculation, see Sec. III) to an $E0$ contribution of $\lesssim 20\%$ of the virtual photon spectrum at 10 MeV excitation. To analyze the data in this region we have used

$$N_{E2}(E_0, E_x) = \frac{\alpha}{\pi}\left[(1+R_E{}^2)\ln\frac{2E_0(E_0-E_x)}{m_e E_x} + R_K{}^2\left(1+\tfrac{5}{3}R_E-\tfrac{25}{12}R_E{}^2\right)\right],$$

where E_0, E_x refer to the incident electron energy and excitation energy, respectively, $R_E = (E_0 - E_x)/E_0$, and $R_K = (E_0 - E_x)/E_x$. The photodisintegration cross section using Eq. (1) is then

$$\left.\frac{d\sigma}{d\Omega}\right|_\gamma = \left(\frac{d^2\sigma}{d\Omega dE}\right)\frac{1}{N_{E2}(E_0, E_x)/E_x}\,\frac{\Delta E_d}{\Delta E_x} ,$$

where

$$E_x = \frac{ME_d + \frac{1}{2}Q(M - M_d + \frac{1}{2}Q)}{M - M_d - E_d + P_d\cos\theta_d} .$$

We point out that this photon spectrum yields es-

sentially the same result for $E_x > 10$ MeV as that obtained when one considers all appropriate multipoles (except $E0$) in the photon spectrum.

III. THEORY

To obtain a qualitative understanding of the measured electrodisintegration cross sections we rely on a simple model for the process. In particular, we assume an α-d cluster model where the intercluster potential is a square well. The well parameters are determined as follows. For the ground state we ask that $R_{1S}(r)$, the *one-node* $l=0$ *wave function*, be bound by 1.474 MeV and the charge radius

$$\langle r^2\rangle_{\rm ch} = \tfrac{2}{3}\langle r^2\rangle_\alpha + \tfrac{1}{3}\langle r^2\rangle_d + \tfrac{6}{27}\int_0^\infty r^4 |R_{1S}(r)|^2 dr$$

be equal to $(2.57)^2$ fm^2. Following the work of Aurdal, Bang, and Hansteen[6] and of Bergstrom and Tomusiak (Ref. 2) we choose $\langle r^2\rangle_\alpha^{1/2} = 1.68$ fm and $\langle r^2\rangle_d^{1/2} = 1.5$ fm.[7] These criteria give the parameters

$$V = -25.43 \text{ MeV}, \quad a = 4.0 \text{ fm},$$

which are used for all partial waves except $l=2$. The $l=2$, α-d channel has three resonances described in this picture by $^3D_3$, $^3D_2$, and $^3D_1$ at excitation energies of 2.183, 4.31, and 5.7 MeV, respectively. This resonance structure could be built into the model by the addition of a spin-orbit force to the $l=2$ potential. For the present, however, we use only a central potential adjusted to give an $l=2$ phase shift resonance of about the correct width at 4.7 MeV. In the more refined model used by Bergstrom and Tomusiak (Ref. 2) the phase shift resonance at 4.7 MeV shows up as a resonance in the ^{6}Li(e, e') reaction at 4.3 MeV. With the present oversimplified model the resonance is shifted down to 3.8 MeV in the photodisintegration cross section. Finally we list our $l=2$ well parameters

$$V_{l=2} = -14.41 \text{ MeV}, \quad a = 4.0 \text{ fm}.$$

The electrodisintegration cross section for measuring only the outgoing deuterons is given by the one-photon exchange approximation by Dressler and Tomusiak[8]

$$\frac{d^2\sigma}{dE_d d\Omega_d} = \frac{4\hbar c\alpha^2}{\epsilon_k}\rho_N \int \frac{\{x\}}{q_\mu^4 \epsilon_{k'} q_0^2}\,\delta(\text{energy})\rho_{e'} d\epsilon_{k'} d\Omega_{k'},$$

where

$$\{x\} = \{[(\epsilon_k \vec{k}' - \epsilon_{k'}\vec{k})\cdot\vec{J}\,]^2 + \tfrac{1}{4}(\hbar c)^2 q_\mu^2 [q_0^2 \vec{J}\cdot\vec{J} - (\vec{J}\cdot\vec{q})^2]\},$$

$$\delta(\text{energy}) = \delta\left(\epsilon_k - \epsilon_{k'} - \frac{\hbar^2 P_d^2}{2M_d} - \frac{\hbar^2 P_\alpha^2}{2M_\alpha} - 1.474\right),$$

$$q_\mu^2 = (\vec{q}^2 - q_0^2) = (\vec{k} - \vec{k}')^2 - \frac{1}{\hbar^2 c^2}(\epsilon_k^2 - \epsilon_{k'}^2),$$

$$\vec{P}_\alpha = \vec{k} - \vec{k}' - \vec{P}_d,$$

$$\rho_N = \rho_d^2 \frac{dP_d}{dE_d} = \frac{M_d P_d}{\hbar^2},$$

and

$$\rho_{e'} = k'^2 \frac{dk'}{d\epsilon_{k'}} \simeq \frac{k'^2}{\hbar c}.$$

If we restrict our attention to $E0$, $E1$, and $E2$ contributions then the nuclear current $\vec{J}$ is given by

$$\vec{J} = \frac{1}{(2\pi^2)^{1/2}}\left(\frac{q_0}{q}\right)[\hat{q}\,\mathcal{R}_0(\kappa, q) + 3\hat{\kappa}\,\mathcal{R}_1(\kappa, q) + \tfrac{5}{2}(3\hat{\kappa}(\hat{\kappa}\cdot\hat{q}) - \hat{q})\mathcal{R}_2(\kappa, q)], \tag{2}$$

where

$$M = M_\alpha + M_d,$$

$$\vec{\kappa} = \frac{M_d}{M}\vec{P}_\alpha - \frac{M_\alpha}{M}\vec{P}_d,$$

$$\mathcal{R}_L(\kappa, q) = \int_0^\infty R_L^*(\kappa, r) M_L(q, r) R_{1S}(r) r^2 dr,$$

and

$$M_L(q, r) = 2f_\alpha(q) j_L\left(\frac{M_d}{M} qr\right) + (-1)^L f_d(q) j_L\left(\frac{M_\alpha}{M} qr\right). \tag{3}$$

The deuteron and α particle form factors are given by

$$f_\alpha(q) = e^{-0.375q^2}$$

and

$$f_d(q) = e^{-0.470q^2}.$$

In the above, $R_L(\kappa, r)$ is the L-wave continuum wave function with asymptotic normalization

$$R_L(\kappa r) \sim \frac{e^{i\delta_L(\kappa)}}{\kappa r}\sin(\kappa r - \tfrac{1}{2}l\pi + \delta_L(\kappa)).$$

Electric dipole transitions are strongly suppressed in this model.[9] From Eq. (3) one can obtain the long wavelength (small q) approximations

$$M_1(q, r) \simeq \frac{2M_d - M_\alpha}{3M} qr \simeq \tfrac{1}{750} qr,$$

$$M_2(q, r) \simeq \tfrac{2}{45} q^2 r^2,$$

and, neglecting a term which does not contribute because of wave function orthogonality,

$$M_0(q, r) \simeq -\tfrac{1}{9} q^2 r^2.$$

Thus only for momentum transfers $\lesssim 0.02$ fm^{-1}

does the $E1$ disintegration become important in comparison to the $E0$ and $E2$ modes.

In discussing our experimental and theoretical electrodisintegration results we will refer to the calculated photodisintegration cross sections. These are calculated with both the square well model described above and with the model used in Ref. 2. That model, which employs a Woods-Saxon well plus the Coulomb potential, includes both 3^+ (2.183 MeV) and 2^+ (4.31 MeV) resonances. We list formulas for the case of a spin-orbit force in the $l=2$ *channel only* so that the $l=2$ continuum wave functions are labeled by $R_{2,J}(\kappa r)$ and the multipole matrix elements by $\mathcal{R}_{2,J}(\kappa, q)$. For other than $l=2$ the notation is that used in Eqs. (2) and (3). The c.m. angular distribution is given by

$$\frac{d\sigma_\gamma}{d\Omega_{\hat{\kappa}}} = \frac{\alpha\kappa}{E_\gamma}\left(\frac{M_\alpha M_d c^2}{M}\right)(A_0 + A_2\sin^2\theta_\kappa + A_3\sin^2\theta_\kappa\cos\theta_\kappa + A_4\sin^2\theta_\kappa\cos^2\theta_\kappa),$$

where

$$A_0 = \tfrac{15}{8}|\mathcal{R}_{21}|^2 + \tfrac{25}{24}|\mathcal{R}_{22}|^2 + \tfrac{25}{6}|\mathcal{R}_{23}|^2 + \tfrac{5}{4}\mathrm{Re}(\mathcal{R}_{22}\mathcal{R}_{21}^*) - \tfrac{10}{3}\mathrm{Re}(\mathcal{R}_{23}^*\mathcal{R}_{22}) - 5\mathrm{Re}(\mathcal{R}_{23}^*\mathcal{R}_{21}),$$

$$A_2 = 9|\mathcal{R}_1|^2 - \tfrac{9}{16}|\mathcal{R}_{21}|^2 + \tfrac{25}{48}|\mathcal{R}_{22}|^2 - \tfrac{23}{12}|\mathcal{R}_{23}|^2 - \tfrac{15}{8}\mathrm{Re}(\mathcal{R}_{22}^*\mathcal{R}_{21}) + \tfrac{5}{6}\mathrm{Re}(\mathcal{R}_{23}^*\mathcal{R}_{22}) + 3\mathrm{Re}(\mathcal{R}_{23}^*\mathcal{R}_{21}),$$

$$A_3 = \mathrm{Re}[\mathcal{R}_1^*(9\mathcal{R}_{21} + 15\mathcal{R}_{22} + 21\mathcal{R}_{23})],$$

$$A_4 = \tfrac{25}{3}|\mathcal{R}_{22}|^2 + \tfrac{55}{12}|\mathcal{R}_{23}|^2 + \tfrac{45}{2}\mathrm{Re}(\mathcal{R}_{23}^*\mathcal{R}_{21}) + \tfrac{125}{6}\mathrm{Re}(\mathcal{R}_{23}^*\mathcal{R}_{22}).$$

In the approximation that $\mathcal{R}_{21}=\mathcal{R}_{22}=\mathcal{R}_{23}=\mathcal{R}_2$, we have

$$A_0 = 0,$$

$$A_2 = 9|\mathcal{R}_1|^2,$$

$$A_3 = 45\,\mathrm{Re}|\mathcal{R}_1^*\mathcal{R}_2|,$$

and

$$A_4 = \tfrac{225}{4}|\mathcal{R}_2|^2.$$

For completeness we list the α-d total photodisintegration cross section

$$\sigma_\gamma = \frac{8\pi}{3}\frac{\alpha\kappa}{E_\gamma}\left(\frac{M_\alpha M_d c^2}{M}\right)[\tfrac{3}{2}A_0 + A_2 + \tfrac{1}{5}A_4].$$

In computing photo cross sections with this model, no weight is given to the $^3D_1$ channel, i.e., the matrix element $\mathcal{R}_{21}$ is set equal to zero. Since this resonance is likely a mixture of $^3S_1$ and $^3D_1$ due to a tensor component in the α-d cluster potential, the $E2$ strength to this resonance is therefore expected to be suppressed. In addition, its contribution is down due to the lower statistical weighting a $J=1$ receives compared to a $J=2$ or $J=3$ level.

IV. RESULTS AND DISCUSSION

The electrodisintegration results, experiment and theory, are shown in Figs. 2 and 3. For $\theta_{\mathrm{lab}} = 45°$ and 87° (these angles respectively maximize and minimize the $E2$ contribution to the cross section) the $E0$ and $E2$ contributions to the cross section are also shown. Several features are immediately noticeable. First, in all the spectra the theory lies appreciably below the experiment for $E_d \lesssim 5$ MeV. This can be explained by noting that only the $l=2$ resonance appears in the square well electrodisintegration theory corresponding to the 4.31 MeV level in ^{6}Li (this resonance ap-

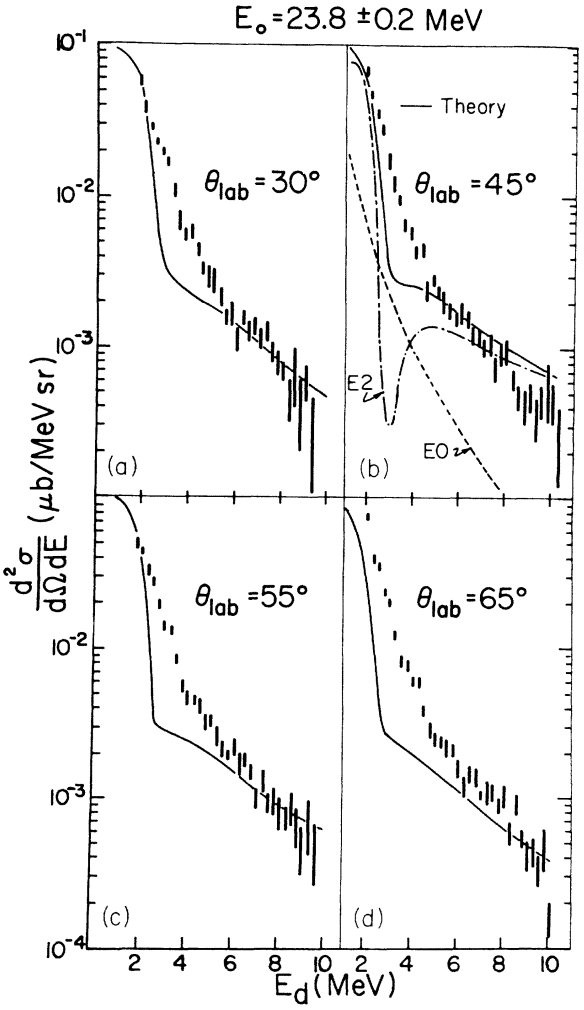

FIG. 2. Electrodisintegration theory and deuteron energy distributions at four laboratory angles for an incident electron energy of 23.8 MeV; (b) shows the $E2$ and $E0$ contributions to the differential cross sections.

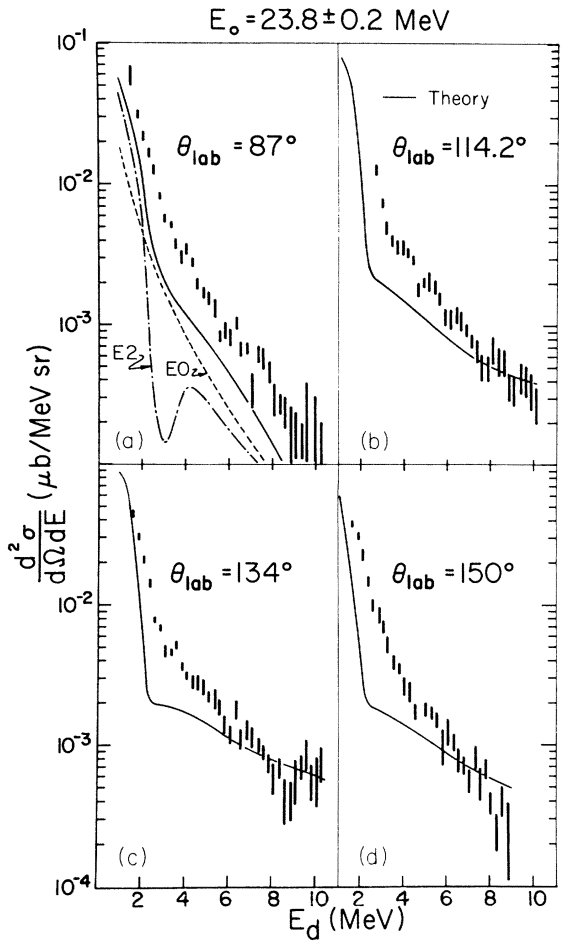

FIG. 3. Electrodisintegration theory and deuteron energy distributions at four laboratory angles for an incident electron energy of 23.8 MeV. (a) shows the $E2$ and $E0$ contribution to the differential cross section.

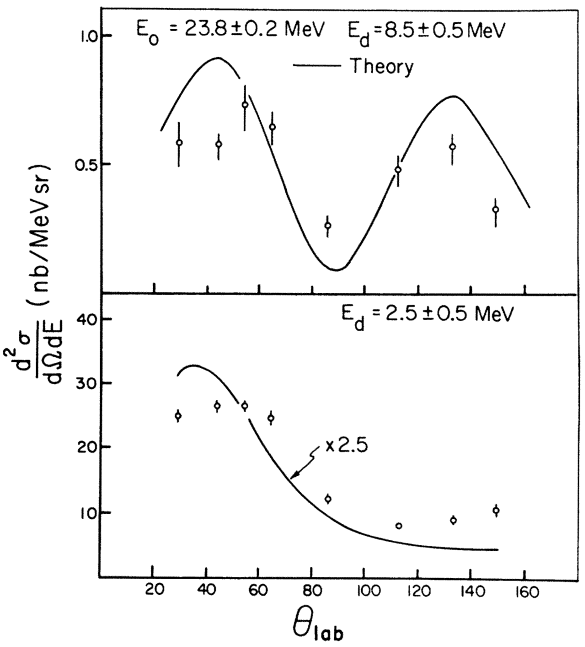

FIG. 4. Angular distribution of deuterons at $E_d = 8.5 \pm 0.5$ MeV and $E_d = 2.5 \pm 0.5$ MeV. The solid line is the electrodisintegration theory described in the text.

pears at a deuteron energy of $E_d \approx 1.9$ MeV). If a spin-orbit force is introduced in the model the contribution to the cross section from the other principal resonance at $E_x = 2.185$ ($E_d \approx 0.5$ MeV) would also be included. The continuum strength of this $^1D_3$ resonance (Ref. 2) would contribute appreciably to the cross section in this energy region.

Yet despite this obvious deficiency in the model one nevertheless still finds the qualitative features of the electrodisintegration data reproduced by the theory. To emphasize this we also show angular distributions sorted in 1 MeV bins at deuteron energies of 2.5 and 8.5 MeV in Fig. 4. The important point is that the shape of the predicted cross section closely resembles the data. Taking note of the fact that the Jacobian which transforms the laboratory cross section to the center of mass is nearly unity for this reaction, we observe that at the lower deuteron energy the monopole contribution which is isotropic and the corresponding interference effects with the odd multipoles are important features of the angular distribution. By examining the individual matrix elements at this energy we find that the $E0$-$E1$ and $E1$-$E2$ interference terms, which have angular dependence in the c.m. system of $\cos\theta$ and $\sin^2\theta\cos\theta$, respectively, are approximately equal. These interference terms are thus undoubtedly responsible for the forward asymmetry at $E_d = 2.5$ MeV since the $E0$-$E2$ interference term varies as $\cos^2\theta$. At $E_d = 8.5$ MeV the $E2$ strength dominates yielding the usual $S \rightarrow D$ quadrupole pattern.

The extracted photodisintegration cross sections are shown in Fig. 5. Here, the model predictions are those of the Woods-Saxon potential with a spin-orbit force that gives the known resonances at 2.185 and 4.35 MeV. As noted in Sec. II we only use the virtual photon analyzed data for $E_x > 10$ MeV because of the extraction dependence on the $E0$ photon spectrum. Again we see reasonable agreement, with the differences between experiment and theory in this case probably explained by the method of data analysis. The angular distribution data, which are more isotropic than the theory, reflects the fact that the monopole was neglected in the virtual photon spectrum. Also,

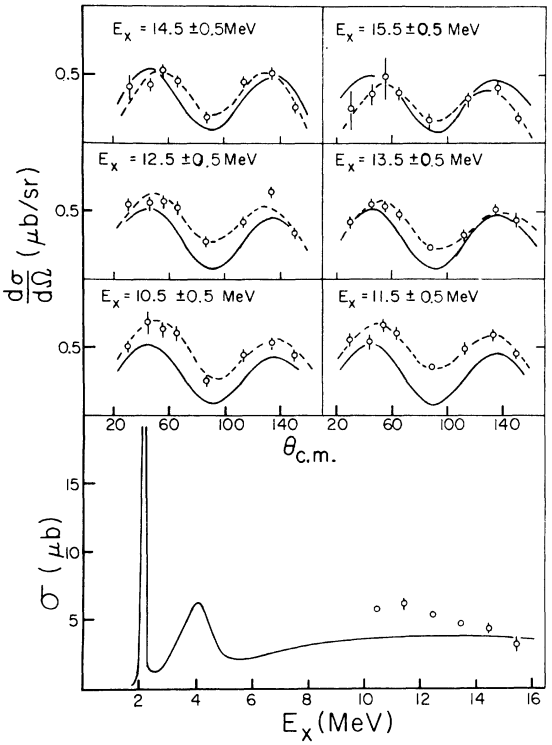

FIG. 5. Extracted photodisintegration cross sections for $E_x > 10$ MeV. The solid curves are the photodisintegration theory described in the text. The dashed lines in the angular distribution data are Legendre polynomial ($l_{max} = 5$) least square fits to the data. The resonance in the total cross section at $E_x = 2.185$ MeV reaches a peak value of 24 μb.

the trend in the total cross section data in this energy range to rise gradually above the theory is expected, since at $E_x = 15.5$ MeV the monopole contribution to the virtual photon spectrum is reduced from the value at 10.5 MeV by ≈60%.

We point out here that as the excitation energy decreases the Woods-Saxon model predicts a pronounced forward asymmetry in the angular distribution data which is due to $E1$-$E2$ interference. The electrodisintegration theory and data as noted earlier also show this effect, but in this case however the forward peaking cannot be solely ascribed to $E1$-$E2$ interference since the $E0$-$E1$ interference term is of comparable strength, while the $E0$-$E2$ interference is essentially symmetric.

V. SUMMARY

Our electrodisintegration experiment appears to be qualitatively consistent with an unsophisticated α-d cluster model. Further refinements of this cluster calculation are needed and the most obvious improvement to the model, the introduction of a spin-orbit force, should lead to better agreement.

The presence of appreciable $E0$ strength greatly complicates the extraction of an equivalent photodisintegration cross section from our electrodisintegration data since the electrodisintegration measurement was not performed in such a manner as to kinematically render small the monopole effects.

†This work was supported by the Atomic Energy Control Board of Canada and the National Research Council of Canada.

[1]F. Ajzenberg-Selove and T. Lauritsen, Nucl. Phys. A227, 1 (1974).

[2]J. C. Bergstrom and E. L. Tomusiak (to be published).

[3]L. Katz, G. A. Beer, D. E. McArthur, and H. S. Caplan, Can. J. Phys. 45, 3721 (1967); Y. M. Shin, D. M. Skopik, and G. D. Wait, Nucl. Instrum. Methods 94, 381 (1971).

[4]K. F. Chong, M. C. Phenneger, Y. M. Shin, D. M. Skopik, and E. L. Tomusiak, Nucl. Phys. A218, 43 (1974).

[5]D. M. Skopik, Y. M. Shin, M. C. Phenneger, and J. J. Murphy, II, Phys. Rev. C 9, 531 (1974).

[6]A. Aurdal, J. Bang, and J. M. Hansteen, Nucl. Phys. A135, 632 (1969).

[7]One expects the deuteron cluster to be more susceptible to distortion effects than the α cluster. Thus one should not expect the deuteron radius in ^{6}Li to be the same as that for a free deuteron. This has been considered in D. R. Thompson and Y. C. Tang, Phys. Rev. C 8, 1649 (1973); D. R. Thompson and Y. C. Tang, Phys. Rev. 179, 971 (1969).

[8]E. T. Dressler and E. L. Tomusiak (to be published).

[9]The long wavelength $E1$ operator vanishes in the approximation that $M_\alpha = 2M_d$. We observe that in an exact many-particle formulation the isoscalar $E1$ operator is proportional to q^3, whereas in the cluster model it depends linearly on q.